Published in final edited form as:
Nat Struct Mol Biol. 2014 March ; 21(3): 282–288. doi:10.1038/nsmb.2769.

More powerful virus inhibitors from structure-based analysis of HEV71 capsid-binding molecules

Luigi De Colibus[#1], **Xiangxi Wang**[#2], **John A. B. Spyrou**[1], **James Kelly**[3], **Jingshan Ren**[1], **Jonathan Grimes**[1,4], **Gerhard Puerstinger**[5], **Nicola Stonehouse**[3], **Thomas S. Walter**[1], **Zhongyu Hu**[6], **Junzhi Wang**[6], **Xuemei Li**[2], **Wei Peng**[2], **David Rowlands**[3], **Elizabeth E. Fry**[1], **Zihe Rao**[2,7], and **David I. Stuart**[1,4]

[1]Division of Structural Biology, University of Oxford, The Henry Wellcome Building for Genomic Medicine, Headington, Oxford, UK

[2]National Laboratory of Macromolecules, Institute of Biophysics, Chinese Academy of Science, Beijing, China

[3]School of Molecular and Cellular Biology, Astbury Centre for Structural Molecular Biology, University of Leeds, Leeds, UK

[4]Diamond Light Sources, Harwell Science and Innovation Campus, Didcot, UK

[5]Department of Pharmaceutical Chemistry, University of Innsbruck, Innsbruck, Austria

[6]National Institutes for Food and Drug Control, No. 2, TiantanXili, Beijing, China

[7]Laboratory of Structural Biology, School of Medicine, Tsinghua University, Beijing, China

[#] These authors contributed equally to this work.

Abstract

Enterovirus 71 (HEV71) epidemics amongst children and infants result mainly in mild symptoms, however, especially in the Asia-Pacific region, infection can be fatal. At present no therapies are available. We have used structural analysis of the complete virus to guide the design of HEV71 inhibitors. Analysis of complexes with four 3-(-4-pyridyl)-2-imidazolidinone derivatives with varying anti-HEV71 activities, pinpointed key structure-activity correlates. We then identified

Correspondence should be addressed to D.I.S. (dave@strubi.ox.ac.uk) or Z.R. (raozh@xtal.tsinghua.edu.cn)..

AUTHOR CONTRIBUTIONS

D.I.S. and Z.R. supervised and coordinated the project. J.W., Z.H., X.L., G.P. and W.P. made samples available. X.W. purified and crystallized the samples and preformed Thermofluor experiments. The GPP ligands were provided by G.P and J.G. L.D.C. designed ALD and NLD and together with J.A.B.S. ran the in-silico docking and analyzed data under the supervision of D.I.S. L.D.C. and T.S.W. soaked crystals for data collection, which was performed by L.D.C., J.A.B.S., J.R. and E.E.F. L.D.C., J.A.B.S., J.R. and D.I.S. contributed to data processing, structure determination and model building. J.K. performed the *in-vitro* $TCID_{50}$ assay and together with N.S. and D.J.R. analyzed the data. L.D.C., E.E.F. and D.I.S. in discussion with J.R., D.J.R. and Z.R. wrote the manuscript and all authors read and approved the manuscript.

ACCESSION CODES

Coordinates and structure factors for the 6 complexes (HEV71–GPP2, HEV71–GPP3, HEV71–GPP4, HEV71–GPP12, HEV71–NLD, HEV71–ALD) have been deposited in the PDB, with accession codes 4CDQ, 4CDU, 4CDW, 4CDX, 4CEY and 4CEW respectively.

COMPETING FINANCIAL INTERESTS

The authors declare no competing financial interests.

Europe PMC Funders Author Manuscripts

additional potentially beneficial substitutions, developed methods to reliably triage compounds by quantum mechanics-enhanced ligand docking, and synthesized two candidates. Structural analysis and *in vitro* assays confirmed the predicted binding modes and their ability to block viral infection. One ligand (IC_{50} = 25 pM) is an order of magnitude more potent than the best previously reported inhibitor, and is also more soluble. Our approach may be useful in the design of effective drugs for enterovirus infections.

The *Picornaviridae* are a large family of pathogens with major impacts on human and animal health. However there are, as yet, no approved therapies for picornavirus infections. The enteroviruses comprise the largest picornavirus genus. Of these enterovirus 71 (HEV71) is perhaps the greatest threat to public health, after human rhinoviruses which are responsible for the majority of cases of the common cold. HEV71 has been identified as responsible for periodic disease outbreaks throughout the world and in recent years there have been regular major epidemics in South Asia. These are associated with outbreaks of mild childhood exanthema, herpangina, and hand, foot and mouth disease, however, especially in the Asia-Pacific region, fatal neurological and cardiovascular disorders can ensue[1]. Picornaviruses are small positive-stranded RNA viruses with non-enveloped icosahedral capsids comprising 60 copies of proteins VP1–4. Proteins VP1–3 each adopt a β-barrel configuration and are arranged with icosahedral symmetry such that VP1 surrounds the 5-fold axes and VP2 and VP3 alternate about the 2 and 3 fold axes (VP4 is internal)[2]. Canyon-like depressions encircling the five-fold axes in enteroviral capsids are frequently the sites of receptor attachment (Fig. 1a). Uncoating, whereby the capsid opens to release the viral genome into the host cell cytosol in order to replicate, is key to picornavirus infection. Like most enteroviruses, HEV71 harbors within its capsid 60 copies of an hydrophobic “pocket factor”, a natural lipid (sphingosine), buried in a pocket lying at the base of the canyon, in the capsid protein VP1 (Fig. 1a). Expulsion of this molecule following binding of the virus to its receptor triggers a cascade of structural rearrangements, which open the capsid to facilitate genome release[3,4]. Since expulsion of the pocket factor is required for infection, a tight replacement binder could be a useful anti-viral acting on the virus capsid. Pleconaril and BTA798 are two examples of several classes of low molecular weight hydrophobic compounds identified[5,6] to inhibit viral uncoating by such stabilization of the capsid[7,8]. Although no anti-picornavirus drug is yet licensed, two have completed phase II clinical trials, Pleconaril and BTA798[9,10]. BTA798, developed by Biota Holdings, continues to show promise for asthmatic patients with rhinovirus infections[10]. Using the skeletons of Pleconaril [11] and related molecules, a novel class of imidazolidinones has been synthesized with anti-HEV71 activity (IC_{50} in the range of 0.001–25μM[12,13]) and the crystal structure of HEV71 particle[4,14,15] now provides an opportunity for the rational improvement of such inhibitors[15]. The use of crystal structures of protein-ligand complexes in combination with *in silico* methods to guide anti-viral inhibitor design is now well established as an effective strategy, with a notable early example being that which led to the first useful anti-influenza virus drug[16]. Nevertheless the use of whole viruses as targets has not been routinely integrated into pharmaceutical pipelines and it is well known that existing *in silico* methods have usually struggled to rank compounds by binding affinity[17].

Europe PMC Funders Author Manuscripts

We set out to design more effective small molecule antivirals targeting HEV71, based on structural information. To this end we analyzed the experimentally derived, high resolution structures of HEV71 bound to four 3-(-4-pyridyl)-2-imidazolidinone derivatives (Fig. 1b)[12] and using robust *in silico* docking methods ranked potential novel inhibitors. We designed a number of compounds, triaged these *in silico* and synthesized two. We used efficient '*in situ*' crystallography[18] to determine inhibited capsid structures, demonstrating that the compounds bound as expected to the virus, and demonstrated that they inhibit infection. One of these compounds is an order of magnitude more potent than the previous best inhibitor.

RESULTS

Structural basis of 3-(4-pyridyl)-2-imidazolidinone activity

We determined the structures of HEV71 in complex with the uncoating inhibitors GPP2, GPP3, GPP4 and GPP12 (3-(-4-pyridyl)-2-imidazolidinone derivatives defined in Figs. 1 and 2, Table 1). Since these, and most pocket factor analogues, are rather insoluble they were dissolved in DMSO before soaking into preformed crystals (see **online Methods**). Data were collected at room temperature in crystallization plates at the Diamond Light Source[18], providing structures at between 2.65 and 2.8 Å resolution (**online Methods** and Table 1). As seen from the electron density maps the compounds replace the natural pocket factor (modeled as sphingosine), with only small shifts (0.1 Å – 0.4 Å) in the backbone of the residues lining the pocket, reflecting their shape similarity with sphingosine (Supplementary Fig. 1). The surface area accessible to solvent, calculated by Areaimol[19], is 8 $Å^2$ for GPP3, 11 $Å^2$ for GPP2, 12 $Å^2$ for GPP4, 9 $Å^2$ for GPP12 and for the natural pocket factor 9 $Å^2$, demonstrating that all of these molecules are essentially fully buried, with GPP3 perhaps inserted slightly deeper into the pocket. All compounds bind with their pyridine ring close to the entrance of the pocket, the carbonyl oxygen of the imidazole moiety hydrogen-bonding to the backbone nitrogen of residue Ile113, as seen with sphingosine, and the phenoxy-ring sandwiched between two phenylalanines (Phe135, Phe155) (Fig. 2). The introduction of a methyl group in the GPP3 linker region results in an order of magnitude tighter binding compared to GPP2 (Fig. 1 and Fig. 3a).

in silico docking

We assembled a database of published inhibition data for 47 HEV71 inhibitors[12,13,20](Supplementary Table 1 and generated correlation plots between the published IC_{50} values[12,13,20] and the energy of interaction computed from their docking poses in the VP1 pocket for Quantum Mechanics Polarised Ligand Docking (QMPLD)[21] implemented in the Schrödinger suite (http://www.schrodinger.com). Several docking methods were tested, for details see Supplementary Note**,** of these the QMPLD[21] method provided a very compelling correlation of 0.81 (Fig. 3b).

The quantum mechanical optimized procedure reliably predicted the experimentally observed poses (Supplementary Fig. 3**)**. In particular the predicted docking poses of GPP2 and GPP3 had root-mean-square deviations (RMSD) of less than 2 Å from the crystal structures (Supplementary Fig. 3). The template structure used for the docking was determined at 2.65 Å resolution and to test the robustness of the method we repeated some

of these experiments using independent structure determinations, both at a similar resolution[15] (2.7 Å) and also at much lower resolution[14](3.7 Å). Results shown in Supplementary Figs. 4 demonstrate that even a rather low resolution structure can accurately reproduce the correct binding mode.

Plate-based inhibitor characterization

Using inhibitors GPP3 and GPP2, we next validated particle thermostability as a measure of compound potency using a plate-based high-throughput thermofluor assay, PaSTRy[22], developed to assess viral stability and the dynamics of uncoating[3,4]. GPV13 (1-[(2-chlorophenoxy)methyl]-4-[(2,6-dichlorophenyl)methoxy]-benzene), a compound similar to SCH47820 which shows strong activity against poliovirus type 2, several echoviruses and Coxsackieviruses, but only weak activity against HEV71[9], was used as a negative control.

The purified virus releases its RNA genome (T_R) at ~58°C, however after incubation with 200 μg/ml GPV13, GPP3 or GPP2 for 72 hours at room temperature the T_R was raised to 60–61°C (Fig. 3c), indicative of a stabilization of the particle. At the lower concentration of 20μg/ml GPP3 and GPP2 still showed increased particle stability after 24 h incubation whereas GPV13 had little effect even after 72 h (Fig.3d). These results are consistent with the EC_{50} values reported for GPP3, GPP2 and GPV13 of 10 nM, 100 nM and 40 μM respectively (the only measured IC_{50}, for GPP2, was 1nM)[12]. Interestingly the protein melting (T_m) of untreated virus occurred in two distinct steps with values of ~58 °C and ~65 °C. Taken together with T_R, this indicates a two-stage transition in protein conformation, with the lower temperature transition corresponding to virus expansion and the release of RNA (Fig. 3e) and the higher temperature the protein melting. In contrast only the higher transition was found after incubation with 200μg/ml GPP3 or GPP2 and the T_m peaks were sharper (Fig. 3f).

Design of potentially improved HEV71 inhibitors

With these tools for assessing *in silico* docking and thermostability we next used the structural data to steer the design of more potent compounds. The binding pocket of HEV71 is more exposed than for most other picornaviruses[4,14]. Based on inspection of the pocket entrance at the bottom of the canyon, we postulated that introducing a functional group such as an amine or amide on the pyridine ring (Fig. 3a) might simultaneously increase the solubility of the compound and enhance its affinity for the virion, by allowing the formation of hydrogen bonds with polar residues (for instance Q202 or D112) (Fig. 3a).

To test this hypothesis, we scanned *in silico* the pocket surface with a collection of probes, using GRID[23] to identify binding hotspots. An amine with a lone pair probe identified a hotspot around the residue D112 with an overall energy of interaction of −15 kcal mol^{-1}. This minimum became more pronounced (−17 kcal mol^{-1}) when the probe was a protonated primary amine. The region around Q202 is also a hotspot for binding the primary amine with interaction energy of −20 kcal mol^{-1} (Fig. 4a). These results support the hypothesis that introducing an amino group on the pyridine ring would increase the overall binding energy due to the formation of a hydrogen bond with residues on the canyon floor. On this basis, modifications of the GPP3 molecule were generated *in silico*, exploring the effect of

multiple substituents on the pyridine ring and replacing the pyridine with alternative moieties of different size. Several dozen possibilities were generated (using PRODRG[24]) and triaged by visual inspection. Some six compounds including furan, isoxazole, pyrrole, and amine-thiazole derivatives were selected to take forward to the next stage of *in silico* ranking and four were chosen to be synthesized. Of these two were produced readily and mass spectrometry confirmed that they were highly pure (Supplementary Fig. 5**)**.

The results of *in silico* docking using the QMPLD method described above (supplementary Methods) for the two molecules synthesized, termed NLD and ALD, are shown in Fig. 4b,c. NLD (molecular weight 448 Da) is a variant of GPP3 where position 2 of the pyridine ring has been replaced with a primary amine (Fig. 4b). The docking poses show this molecule engaged with its amino group forming a hydrogen bond to the carbonyl group of Q202, increasing the number of virus capsid-ligand interactions. To achieve this, docking flips the pyridine ring by 180° compared to its orientation in the HEV71–GPP3 complex. The second molecule, ALD (molecular weight 476 Da), has position 2 of the pyridine ring replaced with an amide (Fig. 4c). The docking pose suggests that this substituent will form hydrogen bonds with the side chain of D112. The predicted IC_{50} values were 2.6 pM and 0.8 pM for NLD and ALD respectively (Fig. 3b). LogP (logarithm of the n-octanol–water partition coefficient) for GPP3 is calculated to be 3.8, whereas for NLD and ALD this decreased to 3.6 and 3.0, respectively, suggesting that these compounds are rather more soluble than previous inhibitors, in addition the theoretical absorption, distribution, metabolism and excretion (ADME-tox) properties (calculated using QickProp v3.6, Schrödinger suite: http://www.schrodinger.com and reported in Supplementary Table 2) appear favourable.

ALD and NLD readily replace the natural pocket factor

To establish if and how ALD and NLD bound they were soaked into HEV71 crystals. The compounds were indeed more soluble than the GPP series and soaking with the protocol used for these led to rapid degradation of the crystals. We therefore reduced the concentration of the compounds 550-fold, allowing diffraction data to be collected and room temperature structures determined at 2.75Å resolution[18]. Both ligands maintain the key useful interactions described above (Fig. 5a,b). The presence of the amide group on the pyridine moiety allows ALD to establish hydrogen bonds with the side chain of D112, exactly as predicted by *in silico* docking (Fig. 5b). However for NLD, the crystal structure shows that the amine group on the pyridine moiety, rather than interacting with the peptide carbonyl moiety of Q202 as predicted by *in silico* docking, is rotated by almost 180° to interact instead with the side chain of D112, in a similar way to that observed for ALD (Fig. 5b). With the exception of this reorientation the experimental results agree with the predicted docking poses (RMSD < 2Å). To investigate the NLD docking, we used program LigPrep (http://www.schrodinger.com) which suggested that at pH 7 the pyridine nitrogen could be protonated. Re-docking NLD with a protonated pyridine produced an essentially correct pose (RMSD 0.5Å *cf* experimental result) of similar energy.

NLD and ALD are powerful HEV71 inhibitors in vitro

PaSTRy analysis confirmed that NLD and ALD are potent capsid stabilizers, enhancing stabilization at modest concentrations compared to known tight binders such as GPP3 (Fig.

5c,d). Quantification for such tight binders is difficult, since the concentrations of binding sites (60 times the virus concentration of 0.2 μM), and competing pocket factor (at least equal to the concentration of binding sites) are far above the binding constant for NLD and ALD. The concentration needed to produce thermal stabilization will therefore underestimate the IC_{50} by orders of magnitude [25]. We therefore also compared the inhibitory activities of ALD and NLD to those of GPP3 and GPP4 by *in vitro* $TCID_{50}$ assay in Vero cells. Ten-fold serial dilutions of virus were used in the presence of different concentrations of the compounds. Control wells were exposed to the equivalent concentration of solvent (DMSO) to ensure no cytopathic effect on uninfected cells or on virus titre. NLD was shown to be the most effective inhibitor with an IC_{50} of ~0.025 nM, inhibiting the viral titre to below 5% at concentrations over 0.05 nM. GPP3 was the next most effective inhibitor, with an IC_{50} of 0.319 nM. ALD has an IC_{50} of 8.54 nM (although the $TCID_{50}$ results suggested a more complex biphasic effect). GPP4 did not display inhibitory effects at concentrations up to 1000 nM (Fig. 5e). Finally a further set of experiments were performed to determine the $TCID_{50}$ for NLD and ALD against the full range of HEV71 subtypes, and against CVA16, a related virus also responsible for HFMD (Supplementary Table 3). Encouragingly the compounds are potent against all of these viruses. As seen in Fig. 3b the measured affinity of NLD is in excellent agreement with that predicted *in silico*, however the affinity of ALD is much weaker than predicted. Whilst it is possible that this reflects an error in the *in silico* predictions, the $TCID_{50}$ results suggested a biphasic effect and it is also possible that there were either off-target effects or metabolism of the compound.

DISCUSSION

It has proved notoriously difficult to find useful therapies for picornaviral infections such as the common cold. At present replacing the hydrophobic pocket factors, expelled from many picornaviruses as they uncoat the genome[4], by more robust binders[26,27] is the most promising point for therapeutic intervention [5,6]. To direct the discovery process we determined crystal structures of HEV71 in complex with four ligands with a broad range of affinities. GPP4, the shortest of the four, only partially occupies the binding pocket and has the poorest EC_{50}. This relationship reveals that there is an optimal drug size, which correlates with the efficiency of binding – molecules of the right length better fill the pocket and are better inhibitors. The inhibitors that satisfy this requirement also offer an aromatic moiety at the correct point to occupy a hydrophobic trap formed by Phe135 and Phe155. Indeed in all crystal structures of picornavirus-inhibitor complexes a pair of hydrophobic residues are found at positions equivalent to those occupied by these aromatic residues in HEV71[28,29]. Thus rhinovirus 14 in complex with Pleconavir[30] and poliovirus 2 in complex with a Shering-Plough compound[31] show the antiviral agent located between the structurally equivalent residues Tyr128 and Tyr152, and Phe134 and Tyr159 respectively (Supplementary Fig. 6). The presence of this hydrophobic trap constrains the extent of penetration of such inhibitors and hence the length of the molecule. Increasing the length of the inhibitor causes a mis-alignment of the phenoxy group with respect to Phe135 and Phe155, decreasing the binding energy and undermining the inhibitory effect. Conversely, in GPP4, where the molecule is shorter (bearing just an iodine atom at position 6 on the

phenoxy group), the trap locks the molecule, resulting in a partially filled cavity (Fig. 2d). Nearby, a methyl group in the linker region of GPP3 in large part fills a hydrophobic sub-pocket, giving it the lowest EC50 value (10 nM). The hydrophobic residues (Phe131, Ala133, Met253) lining the sub-pocket leave some space which could possibly accommodate a slightly bigger substituent (Fig. 3a), however Chang *et al*.[20] have shown that phenyl, dimethyl, ethyl and propyl groups cannot fit, since they decrease the affinity. Similarly in rhinovirus bulkier substituents are unfavorable[32], so a methyl group is probably close to optimal.

We have also demonstrated the utility of an extremely rapid plate-based fluorescence assay for inhibitor binding which replicates the rank order of previously reported *in vitro* assays. In addition by measuring RNA accessibility alongside protein unfolding we have found that potent inhibitors elevate the capsid conformational transition associated with genome release to the point at which the capsid proteins melt.

The QMPLD method[21] provided, with guidance from the observed crystal structures, reliable docking results and predictions of binding strength (correlation coefficient 0.81 against a database of 47 prior results). This method, used with care, predicted correct docking poses using a virus structure determined at only 3.7Å resolution. The power of the method is presumably partly due to the fact it uses quantum mechanics to take into account the ligand polarization of the protein environment during the docking process.

Using experimental structural data together with *in silico* mapping of the pocket entrance for additional polar interactions we designed optimized inhibitors (Fig. 4b,c) bearing hydrophilic substituents, which offered the additional benefit of increasing the solubility[33]. The generated docking poses for two of these, ALD and NLD confirmed additional putative hydrogen bonds with the virus and suggested that they were likely to bind more tightly to HEV71 than any previously reported compounds (Fig. 4b).

ALD and NLD were synthesized and found to be soluble and highly reactive with the virus crystals - replacing the pocket factor very effectively. Both contain flexible linker regions, allowing them to adapt well to the shape of the binding pocket. ALD bound as predicted by QMPLD docking, whilst a portion of NLD assumed an alternative conformation, however careful analysis of the protonation state of the molecule led to a revised docking which recapitulated the observed binding mode. *In vitro* analysis using the PaSTRy assay confirmed that both NLD and ALD are powerful capsid stabilizers, with NLD being more potent than the previous gold standard compound, GPP3 (Fig. 5c,d). IC_{50} values from cell-based assays underlined the extraordinary potency of NLD, protecting cells from HEV71 infection at a concentration of 25 pM (Fig. 5e). Furthermore the compounds showed good activity against all HEV71 subtypes and against CVA16, suggesting that such compounds might be broadly effective against the disease (Supplementary Table 3). This is explained by the conservation of residue Asp112 of VP1, which forms a key interaction, across all these viruses.

In summary using the complete virus capsid as a target, we have used a combined experimental and computational approach, starting from nM prior compound with limited

solubility, to obtain, in a single round of design, a next generation broadly effective, relatively soluble pM inhibitor, with many drug-like properties (the calculated ADME-tox properties of NLD (Supplementary Table 2) indicates that the molecules are predicted to have generally acceptable pharmacokinetic properties). Previous experience shows that such inhibitors can generate drug resistant mutations[34], if this occurs with these compounds more work would be required, perhaps a further round of design to build-in resilience to common mutations (for an example of such an approach see Hopkins *et al*.[35]). In conclusion we propose that the approach we describe might facilitate the design of more efficient inhibitors targeted at other enteroviruses, such as rhinoviruses, poliovirus and Coxsackieviruses.

ONLINE METHODS

Virus purification and crystallization

Cells were cultured and virus stocks prepared and crystallized as described previously[4] in nanoliter vapor diffusion Greiner CrystalQuick X plates[36,37]. Cubic crystals emerged in two weeks. GPP2, GPP3, GPP4 and GPP12 were dissolved in 100% DMSO with concentrations of 19 mg/ml, 18.5 mg/ml, 24mg/ml and 68 mg/ml respectively. GPP3 and GPP2 stock solutions were mixed with Crystal Screen 1 (Hampton Research) condition 13 in the ratio 1:2 and further diluted to give a solution containing ~2mg/ml ligand, ~7% PEG400, 44 mM tri-sodium citrate and 22 mM Tris-HCl (pH8.5). GPP4 and GPP12 stock solutions were diluted 55 times in water supplemented with 18% of condition 13 of Crystal Screen 1 (Hampton Research). About 0.5 µl of this solution was added to the 0.2µl crystallization drops one to two weeks prior to data collection (one week was sufficient to allow binding to the virus). For ALD and NLD the protocol was modified: they were dissolved in 100 % DMSO with concentrations of 140 mg/ml and 260 mg/ml, these solutions were diluted 100 times in 100% DMSO and then further diluted 55 times in water supplemented with 18% of condition 13 of Crystal Screen 1 (Hampton Research). One day of soaking was sufficient to allow full replacement of the pocket factor.

PaSTRy assay

Thermofluor experiments were performed as previously described[22]. 50 µl reactions were set up in a thin-walled PCR plate (Agilent), containing 0.5-1.0 µg of HEV71, 5 µM SYTO9 and 3x SYPROred in PBS (pH 7.4) and the temperature ramped from 25 °C to 99 °C, with fluorescence recorded in triplicate at 1 °C intervals. In order to replace the sphingosine with HEV71 inhibitors completely, different concentrations (20 µg/ml and 200 µg/ml) and incubation times (72 or 24 hours) at room temperature were used. The sphingosine was expected to have a slow off-rate and the assay was performed at equilibrium. 5% DMSO was used throughout. The melting temperature, T_m, was taken as the minimum of the negative first derivative of the curve.

Structure determination

Data were collected *in situ*[4,18], on beamlines I24 and I03 at Diamond light source. Diffraction images of 0.05° or 0.1° rotation were recorded on a Pilatus 6M detector using an unattenuated beam of 0.05×0.05 mm^2 at I24 or 0.10×0.06 mm^2 at I03, with exposure times of 0.1s per image. Due to radiation damage in the microcrystals, data collection was limited

to 3-10 frames per crystal. Data processing was performed using the HKL2000 package[38]. Reflections with fractional partialities of >0.7 or > 0.5 were scaled to full intensity (program POST: D.I.S. and J. Diprose, unpublished program). $\langle I \rangle / \langle \sigma_I \rangle$ was calculated with the ioversigma.py program (http://strucbio.biologie.unikonstanz.de/ccp4wiki/index.php/Calculate_average_I/).

Intensities were converted to structure factor amplitudes with TRUNCATE[39]. All crystals belonged to space group *I*23 with 4 pentamers in the asymmetric unit. The HEV71 model PDBID: 3VBF[4] was subjected to positional and B-factor refinement using strict NCS in CNS.1.3[40]. NCS operators were updated by rigid-body refinement of individual protomers in REFMAC5[41] and recalculated NCS matrices used as constraints with CNS.1.3 [40]. Density modification was performed with CNS.1.3[40] and Parrot[42]. Ligand coordinates were generated with PRODRG[24], restraint dictionaries were generated by GRADE (http://grade.globalphasing.org), PRODRG[24] and XPLO2D[43]. Model building was performed with COOT[44]. Water molecules were modeled into the 3.5σ peaks of an *Fo-Fc* map. Models were validated using Molprobity[45]. 93-97% of the residues were in favoured regions of the Ramachandron plot and less than 1% were outliers. Figures were prepared with PyMOL (Schrödinger, LLC) and Chimera[46] .

Molecular docking and binding energy calculation

GRID calculations[23] were performed with default parameters using as probes an amine and protonated primary amine. For docking calculations the input protein structure comprised a complete icosahedral protomer (VP1-4). Small molecule coordinates were generated by PRODRG[24] and energy minimized using Ligprep in the Schrödinger suite at pH 7.0 using the OPLS_2005 force field[47]. The standard conversion procedure with full hydrogen optimization was applied with the Protein Preparation work-flow. The VP1 binding pocket in the crystal structure in complex with the GPP2 ligand was taken as the receptor structure. These processed coordinates were used for the subsequent grid generation and ligand docking procedures. The docking box was centered on the centroid of the GPP2 molecule with an exhaustive search being performed on a box, generally of 8×8×8Å^3, around this point (the larger volume over which the grid potentials were computed extended beyond the likely positions of any ligand atoms). Default values were used for all other parameters. As positional constraints the hydrogen bond between the imidazole moiety of the GPP2 molecule and the carbonyl group of VP1 Ile 113 was used as well as hydrophobic constraints corresponding to the region identified as a hydrophobic trap. For docking the QMPLD (Quantum Mechanics Polarized Ligand Docking)[21] protocol (Schrödinger suite: http://www.schrodinger.com) was used. The most reliable binding pose for each small molecule was selected on the basis of calculated van der Waals and electrostatic interactions.

Viral Titration experiment and Antiviral Activity assays

HEV71 genotype B2 strain MS742387 was titrated on Vero cells by $TCID_{50}$ assay[48]. Viral samples were serially diluted (10^{-2} to 10^{-9}) and added to Vero cells grown in 96 well plates. Each dilution was replicated 10 times along with two control wells that contained no virus. The concentration of each compound was kept constant in each plate. Plates were incubated

for seven days at 37°C, and then stained with crystal violet and the cytopathic effect (CPE) was evaluated. $TCID_{50}$ values were calculated using the Reed-Muench method[48]. Each experiment was repeated three times.

HEV71 genotype A, B3, C4 and CVA16 genotype A, B were titrated on Vero cells by $TCID_{50}$ assay. Viral samples were serially diluted (10^{-2} to 10^{-9}) and added to Vero cells grown in 96-well plates. Each dilution was replicated 5 times along with two control wells that contained no virus. 100 μM inhibitor stock solutions were serially diluted 2-fold with DMEM containing 2% FBS. In each well, 50 μl of diluted inhibitors was mixed with 50 μl of Enterovirus (HEV71, CVA16) containing 100 $TCID_{50}$ concentration of virus and incubated for 1h at 37 °C. Next 100 μl of the virus/inhibitor mixtures were added into wells containing Vero cells. Control wells were exposed to the equivalent concentration of solvent (DMSO) to ensure no cytopathic effect on uninfected cells or on virus titre. After 3 days, the cells were observed to evaluate the appearance of cytopathic effects (CPE). $TCID_{50}$ values were calculated using the Reed-Muench method (reference 53 in the main text). The IC_{50} values of inhibitor compounds against HEV71, genotype A, B3, C4 and CVA16 genotype A, B were read as the lowest concentrations that could protect >50% cells from CPE.

LogP calculations

LogP values were calculated with Virtual Computational Chemistry Laboratory (http://www.vcclab.org/)[49]

Synthesis of ALD

Methyl4-[3-(5-[4-[(ethoxyimino)methyl]phenoxy]-3-methylpentyl)-2-oxoimidazolidin-1-yl]pyridine-2-carboxylate (45 mg, 0.10 mM, 1.00 equiv), methanol (5 mL), $NH_3.H_2O$ (10 mL) and NH_4Cl (1.7 mg, 0.33 equiv) were placed in a 100-mL 3-necked round-bottom flask. The resulting solution was stirred overnight at 40 °C, and then concentrated under vacuum. The residue was diluted with 15 mL of water. The resulting solution was extracted with 3×10 mL of ethyl acetate and the organic layers combined. The mixture was dried over anhydrous sodium sulfate and concentrated under vacuum. The residue was washed with 2×5 mL of ether/hexane (1:1). This yielded 30 mg of ALD as a white solid.

Synthesis of NLD

A solution of tert-butyl N-[4-[3-(5-[4-[(ethoxyimino)methyl]phenoxy]-3-methylpentyl)-2-oxoimidazolidin-1-yl]pyridin-2-yl]carbamate (200 mg, 0.38 mM, 1.00 equiv) in TFA–CH_2Cl_2 (1:1) (20 mL) was placed in a 50-mL round-bottom flask. The resulting solution was stirred for 6 h at room temperature and then concentrated under vacuum. The crude product was purified by Flash-Prep-HPLC. This yielded 30 mg of NLD as a light yellow solid.

Supplementary Material

Refer to Web version on PubMed Central for supplementary material.

ACKNOWLEDGEMENTS

We thank A. Kotecha for assistance with Diamond data collection and the beamline staff at Diamond light source beamlines I03 and I24 provided expert assistance and advice. GPP and GPV compounds were made by F. Prauchart. Mass Spec analyses were carried out by C. Schofield and P. Abrusci helped with the sigma plot program. Administrative and high performance computing was supported by the Wellcome Trust Core Award Grant Number 090532/Z, and particular help was provided by R. Esnouf. Work was supported by the Chinese National Major Project of Infectious Disease, the Ministry of Science and Technology 973 Project (grant nos. 2011CB910300 and 2014CB542800) and the Major National Science and Technology Programs (grant no. 2012ZX10004701). D.I.S., E.E.F. & T.S.W. are supported by the UK Medical Research Council (G110525, G100099), J.R. by the Wellcome Trust, J.K. by Sanofi Pasteur and L.D.C. by the World Health Organisation. Research leading to these results received funding from the European Union FP7, SILVER grant n° 260644.

REFERENCES

1. MCMINN PC. Enterovirus 71 in the Asia-Pacific region: An emerging cause of acute neurological disease in young children. Neurol J Southeast Asia. 2003; 8:57–63.
2. Rossmann MG, et al. Structure of a human common cold virus and functional relationship to other picornaviruses. Nature. 1985; 317:145–153. [PubMed: 2993920]
3. Ren J, et al. Picornavirus uncoating intermediate captured in atomic detail. Nature communications. 2013; 4:1929.
4. Wang X, et al. A sensor-adaptor mechanism for enterovirus uncoating from structures of EV71. Nature structural & molecular biology. 2012; 19:424–429.
5. Rotbart HA. Treatment of picornavirus infections. Antiviral research. 2002; 53:83–98. [PubMed: 11750935]
6. Tsang SK, et al. A structurally biased combinatorial approach for discovering new anti-picornaviral compounds. Chemistry & biology. 2001; 8:33–45. [PubMed: 11182317]
7. Phelps DK, Post CB. A novel basis of capsid stabilization by antiviral compounds. Journal of molecular biology. 1995; 254:544–551. [PubMed: 7500332]
8. Tsang SK, Danthi P, Chow M, Hogle JM. Stabilization of poliovirus by capsid-binding antiviral drugs is due to entropic effects. Journal of molecular biology. 2000; 296:335–340. [PubMed: 10669591]
9. De Palma AM, Vliegen I, De Clercq E, Neyts J. Selective inhibitors of picornavirus replication. Medicinal research reviews. 2008; 28:823–884. [PubMed: 18381747]
10. Feil SC, et al. An Orally Available 3-Ethoxybenzisoxazole Capsid Binder with Clinical Activity against Human Rhinovirus. Acs Med Chem Lett. 2012; 3:303–307. [PubMed: 24900468]
11. Pevear DC, Tull TM, Seipel ME, Groarke JM. Activity of pleconaril against enteroviruses. Antimicrobial agents and chemotherapy. 1999; 43:2109–2115. [PubMed: 10471549]
12. Shia KS, et al. Design, synthesis, and structure-activity relationship of pyridyl imidazolidinones: a novel class of potent and selective human enterovirus 71 inhibitors. Journal of medicinal chemistry. 2002; 45:1644–1655. [PubMed: 11931618]
13. Ke YY, Lin TH. Modeling the ligand-receptor interaction for a series of inhibitors of the capsid protein of enterovirus 71 using several three-dimensional quantitative structure-activity relationship techniques. Journal of medicinal chemistry. 2006; 49:4517–4525. [PubMed: 16854057]
14. Plevka P, Perera R, Cardosa J, Kuhn RJ, Rossmann MG. Crystal structure of human enterovirus 71. Science. 2012; 336:1274. [PubMed: 22383808]
15. Plevka P, et al. Structure of human enterovirus 71 in complex with a capsid-binding inhibitor. P Natl Acad Sci USA. 2013; 110:5463–5467.
16. von Itzstein M, et al. Rational design of potent sialidase-based inhibitors of influenza virus replication. Nature. 1993; 363:418–423. [PubMed: 8502295]
17. Warren GL, et al. A critical assessment of docking programs and scoring functions. Journal of medicinal chemistry. 2006; 49:5912–5931. [PubMed: 17004707]
18. Axford D, et al. In situ macromolecular crystallography using microbeams. Acta crystallographica. Section D, Biological crystallography. 2012; 68:592–600.

19. Winn MD, et al. Overview of the CCP4 suite and current developments. Acta Crystallogr D. 2011; 67:235–242. [PubMed: 21460441]
20. Chang CS, et al. Design, synthesis, and antipicornavirus activity of 1-[5-(4-arylphenoxy)alkyl]-3-pyridin-4-ylimidazolidin-2-one derivatives. Journal of medicinal chemistry. 2005; 48:3522–3535. [PubMed: 15887961]
21. Cho AE, Guallar V, Berne BJ, Friesner R. Importance of accurate charges in molecular docking: quantum mechanical/molecular mechanical (QM/MM) approach. Journal of computational chemistry. 2005; 26:915–931. [PubMed: 15841474]
22. Walter TS, et al. A plate-based high-throughput assay for virus stability and vaccine formulation. Journal of virological methods. 2012; 185:166–170. [PubMed: 22744000]
23. Goodford PJ. A computational procedure for determining energetically favorable binding sites on biologically important macromolecules. Journal of medicinal chemistry. 1985; 28:849–857. [PubMed: 3892003]
24. Schuttelkopf AW, van Aalten DM. PRODRG: a tool for high-throughput crystallography of protein-ligand complexes. Acta crystallographica. Section D, Biological crystallography. 2004; 60:1355–1363.
25. Kenakin, TP. Pharmacologic Analysis of Drug-Receptor Interaction. Lippincott Raven; 1993. p. 483
26. JosephMcCarthy D, Hogle JM, Karplus M. Use of the multiple copy simultaneous search (MCSS) method to design a new class of picornavirus capsid binding drugs. Proteins. 1997; 29:32–58. [PubMed: 9294865]
27. Joseph-McCarthy D, Tsang SK, Filman DJ, Hogle JM, Karplus M. Use of MCSS to design small targeted libraries: Application to picornavirus ligands. J Am Chem Soc. 2001; 123:12758–12769. [PubMed: 11749532]
28. Hiremath CN, Grant RA, Filman DJ, Hogle JM. Binding of the antiviral drug WIN51711 to the sabin strain of type 3 poliovirus: structural comparison with drug binding in rhinovirus 14. Acta crystallographica. Section D, Biological crystallography. 1995; 51:473–489.
29. Grant RA, et al. Structures of poliovirus complexes with anti-viral drugs: implications for viral stability and drug design. Current biology: CB. 1994; 4:784–797. [PubMed: 7820548]
30. Zhang Y, et al. Structural and virological studies of the stages of virus replication that are affected by antirhinovirus compounds. Journal of virology. 2004; 78:11061–11069. [PubMed: 15452226]
31. Lentz KN, et al. Structure of poliovirus type 2 Lansing complexed with antiviral agent SCH48973: comparison of the structural and biological properties of three poliovirus serotypes. Structure. 1997; 5:961–978. [PubMed: 9261087]
32. Diana GD, et al. A model for compounds active against human rhinovirus-14 based on X-ray crystallography data. Journal of medicinal chemistry. 1990; 33:1306–1311. [PubMed: 2158559]
33. Lipinski CA, Lombardo F, Dominy BW, Feeney PJ. Experimental and computational approaches to estimate solubility and permeability in drug discovery and development settings. Adv Drug Deliver Rev. 1997; 23:3–25.
34. Hadfield AT, et al. Structural studies on human rhinovirus 14 drug-resistant compensation mutants. Journal of molecular biology. 1995; 253:61–73. [PubMed: 7473717]
35. Hopkins AL, et al. Design of non-nucleoside inhibitors of HIV-1 reverse transcriptase with improved drug resistance properties. 1. Journal of medicinal chemistry. 2004; 47:5912–5922. [PubMed: 15537346]

ONLINE METHODS REFERENCES

36. Walter TS, et al. A procedure for setting up high-throughput nanolitre crystallization experiments. I. Protocol design and validation. J Appl Crystallogr. 2003; 36:308–314.
37. Walter TS, et al. A procedure for setting up high-throughput nanolitre crystallization experiments. Crystallization workflow for initial screening, automated storage, imaging and optimization. Acta crystallographica. Section D, Biological crystallography. 2005; 61:651–657.
38. Otwinowski Z, Minor W. Processing of X-ray diffraction data collected in oscillation mode. Method Enzymol. 1997; 276:307–326.

39. French S, Wilson K. On the treatment of negative intensity observations. Acta Cryst. A. 1978; 34:517–525.
40. Brunger AT, et al. Crystallography & NMR System (CNS), A new software suite for macromolecular structure determination. Acta Cryst. D. 1998; 54:905–921. [PubMed: 9757107]
41. Nicholls RA, Long F, Murshudov GN. Low-resolution refinement tools in REFMAC5. Acta crystallographica. Section D, Biological crystallography. 2012; 68:404–417.
42. Cowtan K. Recent developments in classical density modification. Acta crystallographica. Section D, Biological crystallography. 2010; 66:470–478.
43. Kleywegt GJ. Dictionaries for Heteros. CCP4/ESF-EACBM Newsletter on Protein Crystallography. 1995:45–50.
44. Emsley P, Lohkamp B, Scott WG, Cowtan K. Features and development of Coot. Acta crystallographica. Section D, Biological crystallography. 2010; 66:486–501.
45. Chen VB, et al. MolProbity: all-atom structure validation for macromolecular crystallography. Acta crystallographica. Section D, Biological crystallography. 2010; 66:12–21.
46. Pettersen EF, et al. UCSF Chimera--a visualization system for exploratory research and analysis. J. Comput. Chem. 2004; 25:1605–1612. [PubMed: 15264254]
47. Banks JL, et al. Integrated Modeling Program, Applied Chemical Theory (IMPACT). Journal of computational chemistry. 2005; 26:1752–1780. [PubMed: 16211539]
48. Reed LJM. A simple method of estimating fifty percentage endpoints. The American Journal of Hygene. 1938; 27:493–497. H.
49. Tetko IV, et al. Virtual computational chemistry laboratory - design and description. J. Comput. Aid. Mol. Des. 2005; 19:453–463.

Europe PMC Funders Author Manuscripts

Europe PMC Funders Author Manuscripts

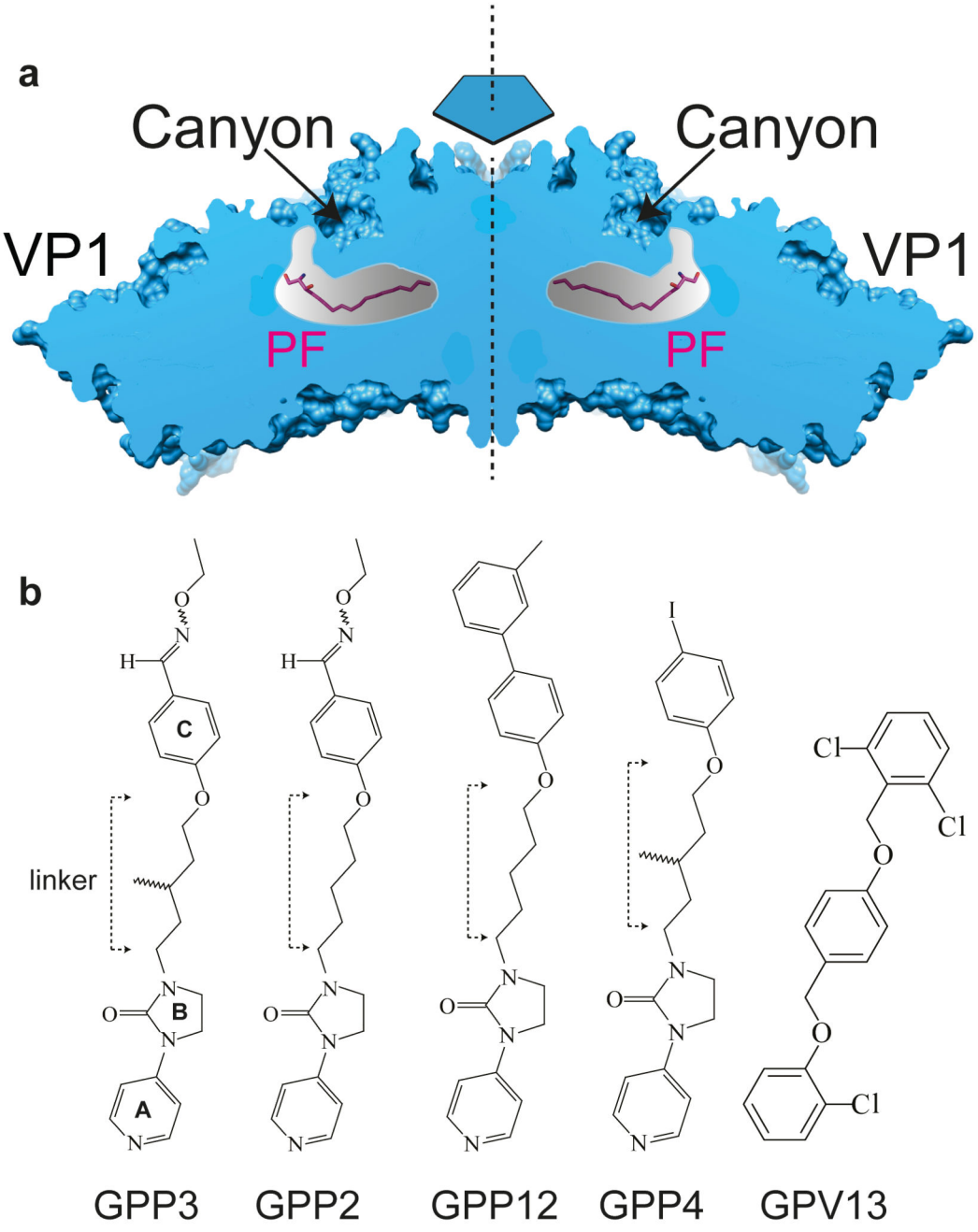

Figure 1. The inhibitor binding site and selected inhibitor structures

(**a**) The organization of the HEV71 inhibitor-binding pocket, lying below the canyon floor, is shown occupied by a natural pocket factor (PF). An icosahedral 5-fold axis is marked. VP1 subunits are shown as a cyan surface. A segment around the 5-fold is cut away to reveal two pockets. (**b**) A selection of 3-(-4-Pyridyl)-2-imidazolidinone derivative structures, ranked according to their EC_{50} value. The EC_{50} for GPP3 is 10 nM, 100 nM for GPP2, 1.3 μM for GPP12, 1.6 μM for GPP4 and 40 μM for GPV013. The following chemical moities are labeled in GPP3: A, pyridine ring; B, imidazole moiety; C, phenoxy group.

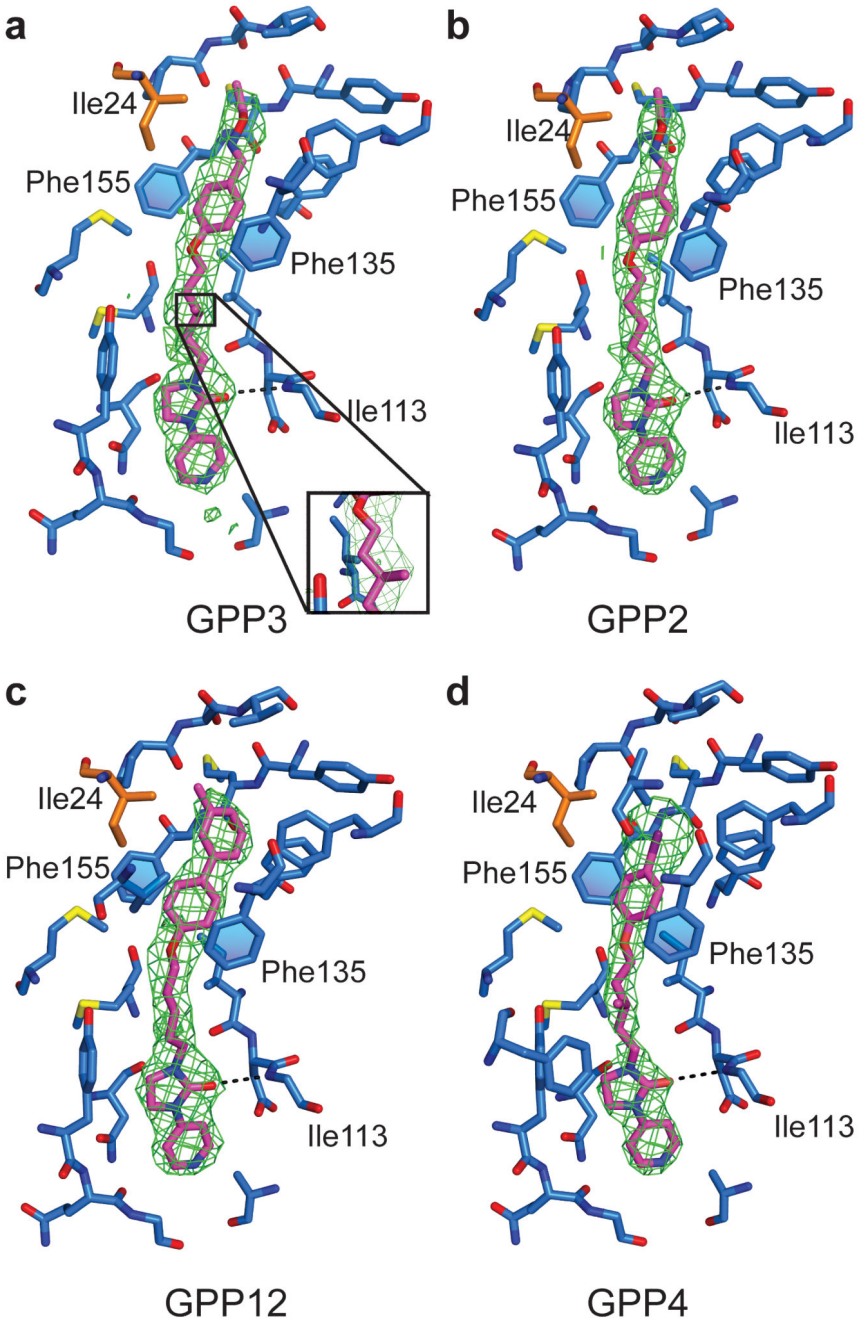

Figure 2. Real-space averaged |*Fo*|–|*Fc*| omit maps (green mesh) of four 3-(-4-Pyridyl)-2-imidazolidinone derivatives bound to HEV71

VP1 residues within 3Å of the ligand are colored in blue and shown in sticks; the side chain of Leu24 of VP3 is colored in orange. The ligands are shown as sticks. (**a,b,c,d**) HEV71–GPP3, HEV71–GPP2, HEV71–GPP12, HEV71–GPP4. Inset in (**a**) shows a close-up view of the methyl group on the GPP3 molecule, the view is rotated by 45° about the y-axis from that in the main illustration.

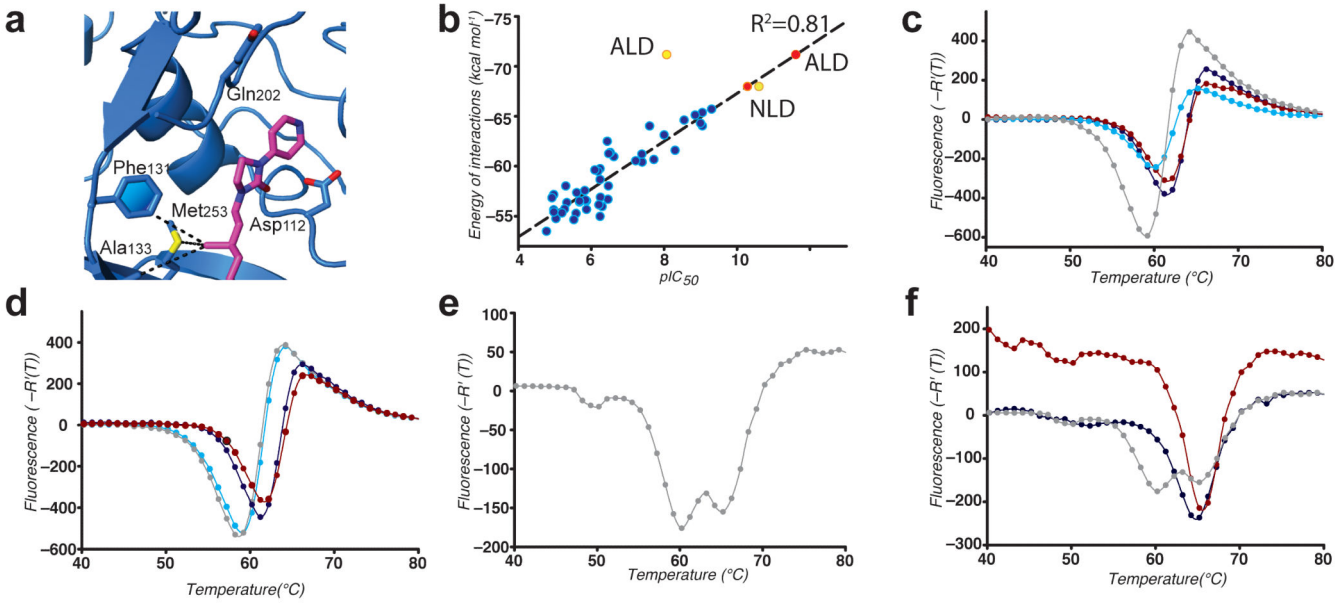

Figure 3. GPP3 bound to VP1 and thermal stabilisation by GPP2, GPP3 and GPV13

(**a**) VP1 is shown as a cartoon (blue), side chains of hydrophilic residues at the pocket entrance and hydrophobic residues surrounding the methyl moiety of GPP3 shown as sticks. Residues contacting the methyl group, are shown: 4.8 Å to Ala133, 4.2 Å to Met253, 4.0 Å to Phe131 Å. (**b**) Correlation plot of binding affinities of 3-(-4-pyridyl)-2-imidazolidinone derivatives predicted by QMPLD *vs* experimental pIC_{50} values. Red dots show the calculated pIC_{50} for the new ligands; experimental values (see below) are in yellow. (**c**) The first derivatives of the fluorescence curves, (see online Methods). Gray line: control virus incubated with dye SYTO9 to detect the release of RNA. Cyan, red and blue lines: HEV71 virions incubated with 200 μg/ml GPV13, 200 μg/ml GPP3 and 200 μg/ml GPP2 respectively with 72 h incubation at room temperature (RT), to which SYTO9 dye has been added. (**d**) results as for (**c**), using SYTO9. The gray line: control virus. The cyan line represents HEV71 virions incubated with 20 μg/ml GPV13 for 72 h at RT and blue and red lines HEV71 virions incubated with 20 μg/ml GPP2 or GPP3 with 24 h incubation at RT respectively. (**e,f**) The first derivative of the fluorescence curve for (**e**) control sample with dye SYPRO RED, to detect protein unfolding and (**f**), gray line is control virus, blue and red lines virions incubated at RT for 72 h with 200 μg/ml GPP2 and GPP3 respectively.

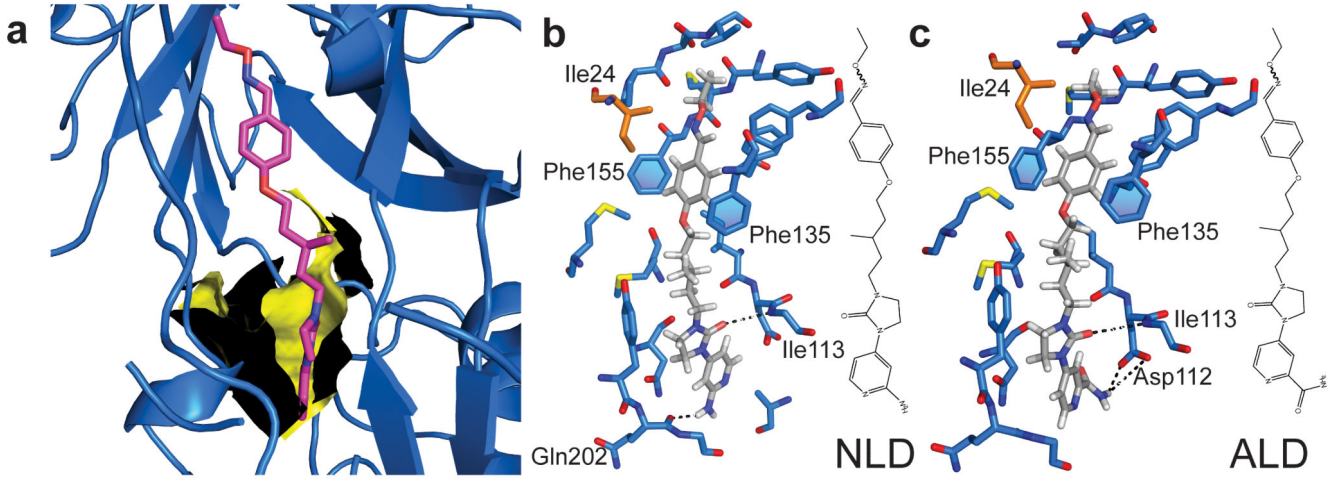

Figure 4. VP1 pocket and docking of the new ligands

(**a**) A GRID map showing the interaction energies between the probe and the explored region within the VP1 binding pocket. The hotspot for binding a primary amine is shown by the yellow surface which is drawn at −15kcal mol^{-1}. (**b**) Molecular docking of NLD, (**c**) and ALD in the VP1 pocket. Both the ligands are shown as sticks. NLD hydrogen bonds with main chain nitrogen of Gln202. ALD establishes hydrogen bond interactions with the side chain of Asp112. The side chain of Ile113 is hidden.

Europe PMC Funders Author Manuscripts

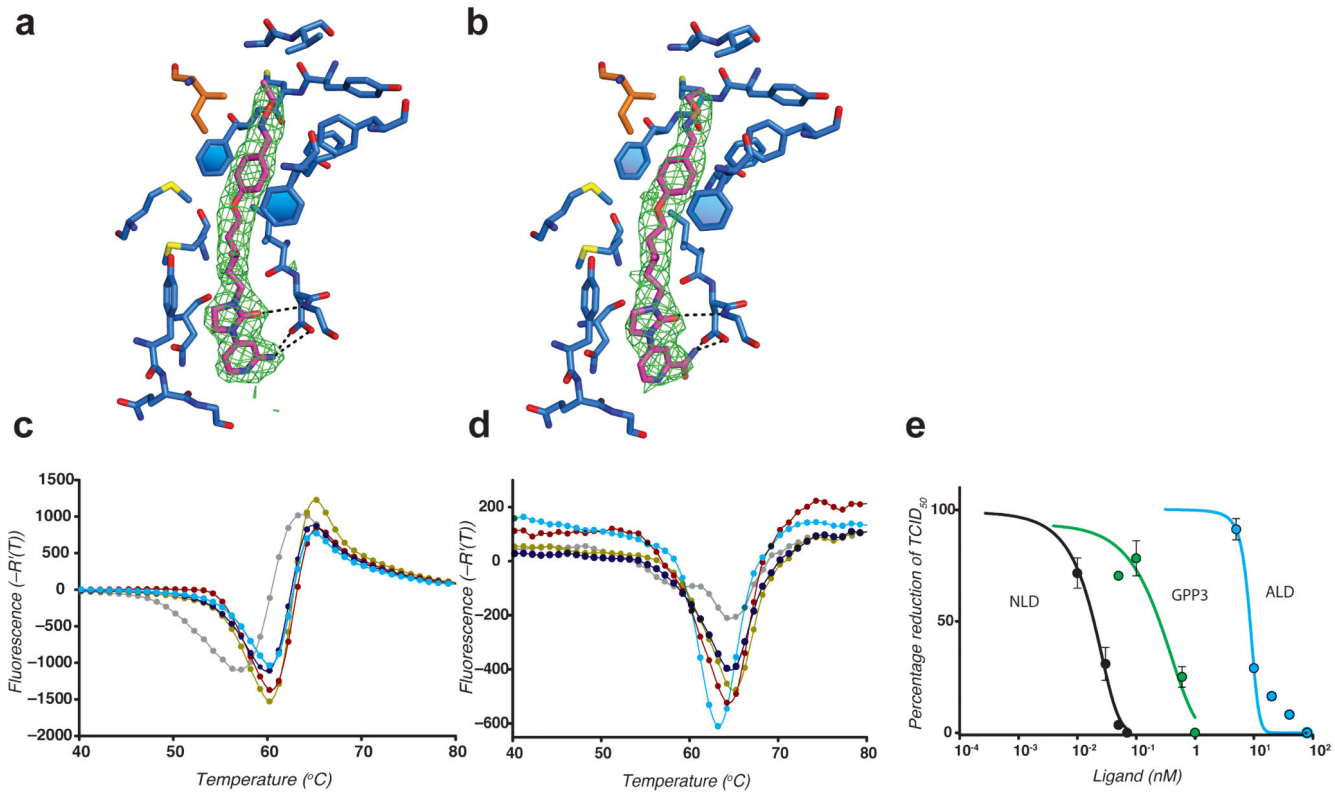

Figure 5. Characterization of newly designed capsid binders bound to the VP1 pocket of HEV71

Crystal structures of the compounds bound to the virus. Single round real space averaged |*Fo*|–|*Fc*| omit maps (green mesh) of (**a**,**b**) NLD ligand in HEV71–NLD complex and ALD ligand in HEV71–ALD complex. (**c**,**d**) First derivatives of the fluorescence curves for the PaSTRy assay. (c) The yellow line represents the control virus incubated with SYTO9 dye, to detect RNA release. The cyan, gray, red and blue lines represent HEV71 virions incubated with 200 μg/ml ALD, NLD, GPP12 and GPP4, respectively, with 24 h incubation at room temperature. (**d**) The yellow line represents the control virus incubated with SYPRO RED, to detect the exposure of hydrophobic protein surfaces. The cyan, gray, red and blue lines represent HEV71 virions incubated with 200 μg/ml ALD, 200 μg/ml NLD, 200 μg/ml GPP12 and 200 μg/ml GPP4, respectively, with 24 h incubation at room temperature. (**e**) HEV71 samples were titrated via $TCID_{50}$ in the presence of a range of concentrations of NLD (black), GPP3 (green) and ALD (cyan). Non-linear regression was used to determine the IC_{50} value. The IC_{50} is the point at which the $TCID_{50}$ value is reduced by 50%. For clarity the curves are represented on a logarithmic scale.

Europe PMC Funders Author Manuscripts

Table 1

Data collection and refinement statistics

	HEV71–GPP2	HEV71–GPP3	HEV71–GPP4	HEV71–GPP12	HEV71–NLD	HEV71–ALD
Data collection						
No. crystals (positions)	38(41)	28(31)	14(17)	13	53(55)	46
Space group	*I23*	*I23*	*I23*	*I23*	*I23*	*I23*
Cell dimensions						
a, *b*, *c* (Å)	*a*=*b*=*c*=599.8	*a*=*b*=*c*=599.7	*a*=*b*=*c*=599.7	*a*=*b*=*c*=599.7	*a*=*b*=*c*=600.3	*a*=*b*=*c*=600.3
Resolution (A)	50.0–2.65 (2.74–2.65	50.0–2.80(2.90–2.80)	50.0–2.80(2.90–2.80)	50.0–2.80(2.90–2.80)	50.0–2.75 (2.85–2.75)	50.0–2.75(2.87–2.75)
R_{merge}	0.488	0.535	0.517	0.539	0.484	0.510
$\langle I/\sigma I \rangle$	2.4(0.8)	1.5(0.5)	1.5(0.5)	1.8(0.6)	1.7(0.7)	1.6(0.6)
Completeness (%)	84.8(57.3)	69.2(30.0)	61.5(59.1)	67.4(66.5)	67.2(57.4)	60.3(49.9)
Redundancy	2.5(1.5)	2.1(1.3)	1.7(1.7)	1.9(1.8)	1.7(1.5)	1.5(1.4)
Refinement						
Resolution (Å)	50.0–2.65	50.0–2.80	50.0–2.80	50.0–2.80	50.0–2.75	50.0–2.75
No. reflections	797,620/41,800	551,890/29,091	478,258/25,074	532,325/27,945	551,343/29,185	494,155/26,036
R_{work} / R_{free}*	0.245/0.246	0.278/0.282	0.283/0.285	0.270/0.272	0.290/0.295	0.302/0.308
No. atoms						
Protein	6506	6506	6506	6506	6506	6506
Ligand/ion	30	33	28	33	33	33
Water	102	63	54	110	60	68
B-factors						
Protein	21	20	25	22	22	19
Ligand/ion/water	17	23	27	19	21	21
R.m.s. deviations						
Bond lengths (Å)	0.008	0.008	0.006	0.007	0.009	0.007
Bond angles (°)	1.5	1.5	1.4	1.4	1.5	1.4

*Note that the R_{free} is of limited significance owing to the considerable non-crystallographic symmetry.

*Values in parentheses are for highest-resolution shell.